Identification and structural characterization of a novel acetyl xylan esterase from *Aspergillus oryzae*

Chihaya Yamada[1], Tomoe Kato[2], Yoshihito Shiono[2], Takuya Koseki[2] (iD) and Shinya Fushinobu[3,4] (iD)

1 School of Agriculture, Meiji University, Kawasaki, Japan
2 Faculty of Agriculture, Yamagata University, Tsuruoka, Japan
3 Department of Biotechnology, The University of Tokyo, Japan
4 Collaborative Research Institute for Innovative Microbiology, The University of Tokyo, Japan

Acetyl xylan esterase plays a crucial role in the degradation of xylan, the major plant hemicellulose, by liberating acetic acid from the backbone polysaccharides. Acetyl xylan esterase B from *Aspergillus oryzae*, designated *Ao*AxeB, was biochemically and structurally investigated. The *Ao*-AxeB-encoding gene with a native signal peptide was successfully expressed in *Pichia pastoris* as an active extracellular protein. The purified recombinant protein had pH and temperature optima of 8.0 and 30 °C, respectively, and was stable up to 35 °C. The optimal substrate for hydrolysis by purified recombinant *Ao*AxeB among a panel of α-naphthyl esters was α-naphthyl acetate. Recombinant *Ao*AxeB catalyzed the release of acetic acid from wheat arabinoxylan. The release of acetic acid from wheat arabinoxylan increased synergistically with xylanase addition. No activity was detected for the methyl esters of ferulic, *p*-coumaric, caffeic, or sinapic acids. The crystal structures of *Ao*AxeB in the apo and succinate complexes were determined at resolutions of 1.75 and 1.90 Å, respectively. Although *Ao*AxeB has been classified in the Esterase_phb family in the ESTerases and alpha/beta-Hydrolase Enzymes and Relatives (ESTHER) database, its structural features partly resemble those of ferulic acid esterase in the FaeC family. Phylogenetic analysis also indicated that *Ao*AxeB is located between the clades of the two families. Docking analysis provided a plausible binding mode for xylotriose substrates acetylated at the 2- or 3-hydroxy position. This study expands the current knowledge of the structures of acetyl xylan esterases and ferulic acid esterases that are required for complete plant biomass degradation.

Introduction

Xylans are the primary constituents of hemicelluloses and, after cellulose, are the second most abundant renewable polysaccharide in lignocellulosic biomass. Xylans conventionally contain heterogeneous substituents, such as arabinose, 2- and 3-*O*-acetyl groups, ferulic (4-hydroxy-3-methoxycinnamic), *p*-coumaric (4-hydroxycinnamic), and 4-*O*-methylglucuronic acids [1]. Acetyl xylan esterases (AXEs, EC 3.1.1.72) hydrolyze ester linkages to release acetic acid from acetylated xylans [2–4], whereas ferulic acid esterases (FAEs, EC 3.1.1.73) hydrolyze ester-linked ferulic acids. Most of the carboxylesterases adopt the α/β-hydrolase fold as a versatile scaffold and have a Ser-His-Asp (or Glu) catalytic triad or a Ser-His catalytic dyad in their active sites for the catalytic mechanism using Ser as the nucleophile [5]. The ESTerases and alpha/beta-Hydrolase Enzymes and Relatives (ESTHER) database is dedicated to the α/β-hydrolase fold enzymes and currently classifies 248 subfamilies [6]. Various types of esterases are listed in ESTHER, including cholinesterases. AXEs are classified into six families (Esterase_phb, FaeC, Antigen85c, Cutinase_like, Acetyl-esterase_deacetylase, and Abhydrolase_7) in the ESTHER database (Table 1). AXEs belong to nine carbohydrate esterase (CE) families (CE1–CE7, CE12, and CE16) in the Carbohydrate-Active enZymes (CAZy) database [7]. CAZy is a database that mainly classifies enzymes that cleave or elongate glycosidic bonds, such as glycoside hydrolases (GHs) and glycosyltransferases, while esterases that cleave acetyl groups and ferulic acid, which modify carbohydrates, are classified in the CE family. Both ESTHER and CAZy classify families primarily according to amino acid sequence similarity, but the range of covered enzymes differs. Many characterized AXEs and FAEs belong to CE1 in CAZy [8], and further subfamily classifications of fungal CE1 have been proposed [9]. According to the CAZy database classification, the AXEs from *Aspergillus* spp. belong to CE1 [10–13] and CE16 [14]. AXEs in CE2, CE3, CE6, CE12, and CE16 do not harbor the α/β-hydrolase fold and are classified into the SGNH hydrolase subfamily of the GDSL family [15], which has a conserved GDSL motif around the nucleophilic serine residue instead of the canonical GxSxG motif present in other serine esterases [16]. Several crystal structures of bacterial SGNH-type AXEs belonging to CE2 and CE3 have been solved to date [17,18]. On the other hand, although many fungal AXEs have been characterized [9–12,19], the crystal structure has been reported only for *Aspergillus luchuensis* AXE A (*Al*AxeA) that is classified into Esterase_phb and CE1 families [20].

In the present study, we identified a new esterase from *Aspergillus oryzae* that has low sequence similarity to characterized AXEs. Gene AO090005000945 from *A. oryzae* encodes a hypothetical protein in the GenBank database (accession number XP_001817948.1).

Table 1. ESTHER families and other family classifications of α/β-hydrolase fold enzymes.

Block[a]	ESTHER rank 1[a]	CAZy[b]	SF[c]	Activities[d]	Member[e]
X	Esterase_phb	CE1	SF6	PHB depolymerase, AXE, FAE	**AsFaeE**, **AlAxeA**, **LtPHBase**, **AoAxeB**
	FaeC	(CE1)[f]	SF5	FAE, AXE	**AaFaeD**, *Ao*AxeC, *Ao*FaeD
	Antigen85c	(CE1)[f]	NL	FAE, AXE	**CtFae-XynY** [30]
	Cutinase_like	CE5	NL	Cutinase, AXE	*Fusarium solani* cutinase [52], *Penicillium purpurogenum* AXEII [53], **TrAxe1** [31]
	Acetyl-esterase_deacetylase	CE7	NL	AXE/CAH	*Bacillus pumilis* AXE/CAH [54]
	Abhydrolase_7	NL	NL	AXE (putative)	*Bacteroides* putative AXEs
	Abhydrolase_5	NL	NL	Undefined	**TmEstA**, LC-Est1, *Ho*Est
	Tannase	NL	SF1	Tannase, FAE, MHETase	**AoFaeB**, *Aspergillus oryzae* tannase [55], *Ideonella sakaiensis* MHETase [56]
	Abhydrolase_6	NL	NL	FAE, lipase	Est1E [57]
L	Lipase_3	NL	SF7	FAE	**AnFaeA** [33]
	Polyesterase-lipase-cutinase	NL	NL	PETase, cutinase	*I. sakaiensis* PETase [56]
H	Tannase_Bact	NL	NL	Tannase	*Lactobacillus plantarum* tannase [58]

[a]ESTHER hierarchically classifies the α/β-hydrolase fold enzymes in the order of Block, Rank 1, and Rank 2 [6]. Block and Rank 1 family are shown; [b]CAZy family [7]. CE1 family is more diverse than the ESTHER families, and not all enzymes are listed; [c]Fungal FAE subfamily proposed by Dilokpimol *et al.* [59]. NL, not listed; [d]Enzymes involved in the degradation of polysaccharides and other polymers are listed. AXE/CAH, acetyl xylan esterase/cephalosporin acetyl hydrolase; MHETase, mono-((2-hydroxyethyl)terephthalic acid) hydrolase, PETase, poly(ethylene terephthalate) hydrolase; PHB depolymerase, poly(3-hydroxybutyrate) depolymerase; [e]Members shown in Figs 5 and 7 are highlighted in bold; [f]Most members are not listed in CAZy, but only a few are classified in the CE1 family.

Table 2. A selection of fungal AXEs and FAEs showing amino acid sequence similarity to *Ao*AxeB. Biochemically characterized enzymes are indicated by their abbreviated names in brackets. The protein sequences from *Aspergillus flavus*, *Aspergillus clavatus*, and *Aspergillus glaucus* are noncharacterized putative enzymes.

Strain	GenBank accession no.	Identity (%)	Similarity (%)
A. flavus	XP_041140962.1	99.6	100
A. clavatus	XP_001272307.1	73.2	92.9
A. glaucus	XP_001817948.1	62.1	93.0
A. oryzae (*Ao*AxeC)	XP_023090471.1	24.5	67.4
T. funiculosus (*Tf*FaeA)	CAC85738.1	24.1	61.5
A. sydowii (*As*FaeE)	XP_040699905.1	20.4	68.5
A. oryzae (*Ao*FaeD)	XP_001823665.1	19.4	58.2
A. oryzae (*Ao*AxeA)	XP_001826329.1	16.7	64.2
A. luchuensis (*Al*AxeA)	BAA13434.1	6.7	50.0

Here, we report the identification and characterization of a novel AXE, designated *Ao*AxeB. We determined the crystal structure of *Ao*AxeB to investigate the structural basis of the classification and catalysis of this enzyme.

Results and Discussion

Expression of *AoaxeB* gene and purification of recombinant *Ao*AxeB

A comparison of the amino acid sequence of *A. oryzae* ORF AO090005000945, provisionally named *AoaxeB*, with the protein database revealed higher sequence identity to hypothetical proteins from *Aspergillus flavus*, *Aspergillus clavatus*, and *Aspergillus glaucus* (Table 2). Low sequence identity (< 25%) was observed with characterized AXEs or FAEs belonging to the FaeC and Esterase_phb families in the ESTHER database: *A. oryzae* AXE C (*Ao*AxeC) [19], *Talaromyces funiculosus* FAE A (*Tf*FaeA), and *A. oryzae* FAE D (*Ao*FaeD) [21] in FaeC, and *A. oryzae* AXE A (*Ao*AxeA) [11] and *Al*AxeA [20] in Esterase_phb. Despite its low sequence similarity, AO090005000945 is currently listed as a putative enzyme (ID: aspor-q2ur69) in the Esterase_phb family, in which AXE, FAE, and poly(3-hydroxybutyrate) depolymerase are classified. The CAZy database does not list this ORF within the CE families.

Aspergillus oryzae ORF AO090005000945, including the original signal sequence, was successfully engineered for protein expression in the heterologous host *Pichia*
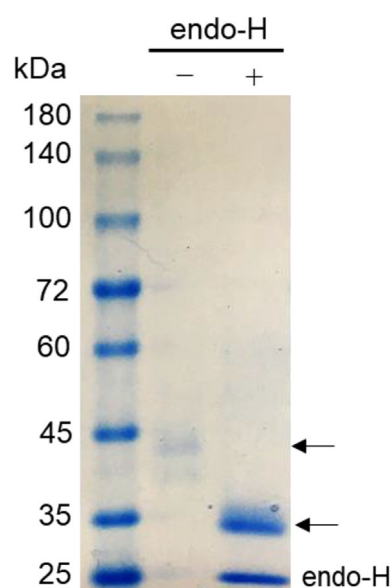

Fig. 1. Coomassie-stained SDS-PAGE of purified *Aspergillus oryzae* acetyl xylan esterase B (*Ao*AxeB). Lane 1, molecular mass markers; lane 2, purified *Ao*AxeB; and lane 3, Endo-H-treated *Ao*AxeB. Arrows indicate the positions of the recombinant protein before (top) and after (bottom) Endo-H treatment.

pastoris. The recombinant protein of *Ao*AxeB was secreted into the medium as an active enzyme and purified using a two-step procedure involving anion exchange and gel filtration chromatography. Purified *Ao*AxeB before and after treatment with endo-β-*N*-acetylglucosaminidase H (Endo-H) migrated in dodecyl-sulfate polyacrylamide gel electrophoresis (SDSPAGE) with a molecular mass of approximately 43 and 34 kDa, respectively (Fig. 1), suggesting that the enzyme possessed *N*-linked oligosaccharides. The NetNGlyc 1.0 server [22] predicted that two putative sites (N42 and N48) in the *Ao*AxeB protein are *N*-glycosylated whereas the other two sites (N295 and N321) are not.

General properties of the purified *Ao*AxeB

The optimum pH of purified *Ao*AxeB was 8.0 with α-naphthyl acetate (C2) as the substrate (Fig. 2A), indicating that *Ao*AxeB had a higher optimum pH than *Ao*AxeA and *Ao*AxeC [12,19]. The optimum temperature for *Ao*AxeB activity was 30 °C. Thermal stability studies ranging 25–50 °C were performed in 50 mᴍ sodium phosphate buffer (pH 8.0) (Fig. 2B). *Ao*AxeB was stable up to 35 °C. However, the thermal stability decreased to 50% of residual activity for 1 h incubation at 40 °C and lost the activity for 1 h incubation at 50 °C. Recombinant *Ao*AxeA was stable up to 40 °C and maintained the activity of approximately
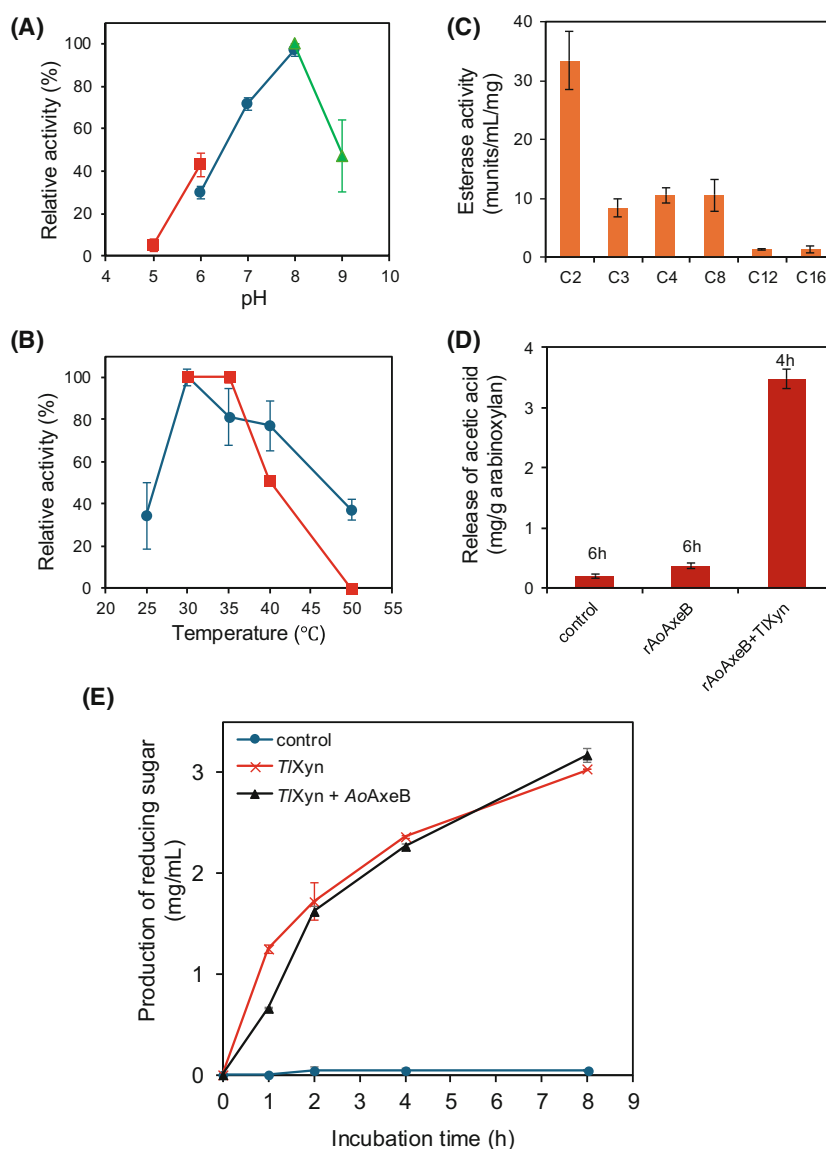
Fig. 2. Biochemical properties of *Ao*AxeB. Data are presented as the mean values of two independent experiments ± standard deviation. (A) Effects of pH on activity. Enzyme activity was measured in citrate buffer (pH 5–6) (red closed squares), phosphate buffer (pH 6–8) (blue closed circles), and Tris/HCl buffer (pH 8–9) (green closed triangles) at 30 °C using α-naphthyl acetate as a substrate. (B) Effects of temperature on activity (blue closed circles) and stability (red closed squares). Enzyme activity was measured in phosphate buffer (pH 8) at different temperatures. For the stability assay, aliquots of purified *Ao*AxeB were incubated for 1 h at different temperatures. After cooling on ice, residual enzyme activity was measured at pH 8.0. (C) Substrate specificity measured using different acyl chain α-naphthyl esters (C2–C16) as chromogenic substrates. Observed maximum activity was set at 100%. (D) Activity toward acetylated xylan. An enzyme-free condition was used as a control. Release of acetic acid from insoluble wheat arabinoxylan was determined as described in the Materials and methods section. (E) Effect of *Ao*AxeB on the production of reducing sugar derived from arabinoxylan degradation by *Thermomyces lanuginosus* xylanase (*Tl*Xyn). The amount of reducing sugar was determined using 2,4-dinitrosalicylic acid. Symbols: blue closed circles, nontreated arabinoxylan; red cross marks, treated arabinoxylan with *Tl*Xyn; black closed triangles, treated arabinoxylan with *Tl*Xyn plus *Ao*AxeB.

20% for 1 h incubation at 50 °C [12]. Meanwhile, recombinant *Ao*AxeC was stable up to 50 °C with a half-life of approximately 2 h at 50 °C and 40 min at

60 °C [19]. The thermal stability of *Ao*AxeB was significantly lower than those of *Ao*AxeA and *Ao*AxeC.

Substrate specificity

The hydrolytic activity of the purified recombinant *Ao*AxeB was examined using a panel of α-naphthyl esters (C2–C16) as artificial substrates. The optimal substrate for *Ao*AxeB was α-naphthyl acetate (C2), and it showed lower activity toward acyl chain substrates containing three or more carbon atoms (Fig. 2C). The specific activity of *Ao*AxeB toward the C2 substrate (0.033 ± 0.005 units·mg^{-1} protein) was threefold higher than that toward α-naphthyl butyrate (C4, 0.011 ± 0.001 units·mg^{-1} protein). Meanwhile, the specific activity of *Ao*AxeC toward C4 (0.10 ± 0.0003 units·mg^{-1} protein) was twofold higher than that toward C2 (0.054 ± 0.005 units·mg^{-1} protein) [19]. This result suggests that *Ao*AxeB shows a higher specificity for acetic acid esters than *Ao*AxeC [19], although the specific activity of *Ao*AxeB is lower than that of *Ao*AxeC. The K_m and k_{cat} values toward the C2 substrate were 0.24 ± 0.12 mм and 0.17 ± 0.03 s^{-1} for *Ao*AxeB and 1.9 ± 0.4 mм and 4.5 ± 0.7 s^{-1} for *Ao*AxeC, respectively. Therefore, the catalytic efficiency (k_{cat}/K_m) for *Ao*AxeB (0.72 s^{-1}·mм$^{-1}$) was lower than that for *Ao*AxeC (2.4 s^{-1}·mм$^{-1}$). Methyl ferulate, methyl *p*-coumarate, methyl caffeate, and methyl sinapate were not hydrolyzed, suggesting that *Ao*AxeB did not show FAE activity.

Release of acetic acid from acetylated xylan and synergism with xylanase

When *Ao*AxeB was incubated with wheat arabinoxylan at 37 °C for 6 h, the amount of released acetic acid (0.37 ± 0.04 mg·g^{-1} substrate) increased by 1.85-fold compared to the enzyme-free condition (0.20 ± 0.04 mg·g^{-1}) (Fig. 2D). A combination of *Ao*AxeB and *Thermomyces lanuginosus* xylanase (*Tl*Xyn), which belongs to GH family 11 (GH11) [23], considerably released acetic acid (3.48 ± 0.16 mg·g^{-1} substrate) at 37 °C for 4 h. Thus, the amount of acetic acid released during a shorter incubation with the xylanase was 9.5-fold the amount released during the incubation with *Ao*AxeB alone. GH11 xylanases have very low activity toward acetylated xylan and produce longer xylooligomers than GH10 xylanases [24]. Thus, the deacetylation of the xylan polymer by *Ao*AxeB may have increased the xylan cleavage activity of *Xl*Xyn, and the released xylooligomers were further deacetylated by *Ao*AxeB. This synergistic effect suggests that *Ao*AxeB is more active against xylooligomers than xylan polymers. In contrast, *Ao*AxeC acts directly on the acetylated xylan polymer [19]. However, no significant synergistic effect of *Ao*AxeB was observed in the degradation of wheat arabinoxylan by *Tl*Xyn (Fig. 2E). In contrast, the release of acetic acid from xylan increased synergistically upon the addition of xylanase to *Ao*AxeA [12].

Crystal structure

The crystal structures of recombinant *Ao*AxeB were determined in apo and succinate complex forms at 1.75 and 1.90 Å resolutions, respectively (Table 3). The crystals of both structures contained one molecule of *Ao*AxeB in the asymmetric unit. The PISA server [25] predicted that the biological assembly in the solution was a monomer. Figure 3A shows the overall structure of the succinate complex form. A clear electron density map of the succinate molecule was observed at the active site (Fig. 3B), where the apo structure contained water molecules (Fig. 3C). The succinate molecule may have been derived from trace contamination in the acetate reagent used for crystallography or the fermentation product of *P. pastoris* used for recombinant protein production because we did not use succinate in the crystallization solution. An acetate molecule was observed on the protein surface because sodium acetate buffer (100 mм) was used in the crystallization solution (Fig. 3A). The apo and succinate complex structures are similar. The root mean square deviations (RMSD) between the two structures was 0.13 Å for 253 over 298 Cα atoms, and there was no structural difference near the active site. However, there is a structural difference far from the active site (Fig. 4A,B). Due to crystal packing, two loops connecting the three β-strands at the edge of the central β-sheet were deviated. The structure predicted using AlphaFold was closer to the apo form (Fig. 4C,D).

*Ao*AxeB consists of a single domain adopting a typical α/β-hydrolase fold, in which a 10-stranded β-sheet is sandwiched by several helices (Fig. 3A). There were three disulfide bonds (C24–C137, C160–C196, and C187–C227). Because we used a protein sample treated with Endo-H, a single *N*-acetylglucosamine was observed at the N-glycosylation sites. The apo structure was N-glycosylated at N42, N248, and N295 (Fig. 4A), whereas the succinate complex contains two N-linked glycans at N42 and N295 (Fig. 4B). This observation partly contradicts the NetNGlyc prediction, where only N42 and N248 are likely N-glycosylation sites.

The catalytic triad is located at the center of the molecule and consists of S149, H282, and D213 (Fig. 3B). The succinate molecule was bound to the active site through numerous hydrophilic interactions. One carboxy group forms direct hydrogen bonds with the side chains of K78, K148, and H282 and a water-mediated hydrogen bond with D292. The other carboxy group

Table 3. Crystallographic data collection and refinement statistics.

	*Ao*AxeB apo	*Ao*AxeB + succinate
Data collection[a]		
Beamline	KEK PF BL5A	SLS PSI X06DA
Wavelength (Å)	1.000	1.000
Space group	$P2_12_12_1$	$P2_12_12_1$
Unit cell (Å)	a = 57.614, b = 63.529, c = 83.417	a = 57.027, b = 64.008, c = 83 324
Resolution (Å)	47.41–1.75 (1.80–1.75)	47.06–1.90 (1.95–1.90)
Total reflections	207 748 (10 264)	133 539 (2020)
Unique reflections	31 605 (1710)	23 666 (1011)
R_{merge}	0.117 (0.859)	0.086 (0.219)
R_{pim}	0.049 (0.379)	0.037 (0.176)
Mean $I/\sigma(I)$	12.1 (2.1)	13.7 (4.1)
$CC_{1/2}$	0.998 (0.713)	0.994 (0.715)
Completeness (%)	100.0 (100.0)	96.0 (65.8)
Multiplicity	6.6 (6.0)	5.6 (2.0)
Wilson B-factor (Å^2)	9.60	11.56
Refinement		
Resolution (Å)	45.45–1.75	47.10–1.90
Reflections	31 549	23 621
R_{work}/R_{free}	0.164/0.199	0.165/0.199
Number of atoms		
Amino acids	2318	2307
Ions	1 (K$^+$)	0
Ligands	52 (1 PGE, 3 NAG)	40 (1ACT, 1SIN, 2NAG)
Waters	323	245
Glycosylation	N42, N248, N295	N42, N295
Average B-factor (Å^2)		
Protein	17.28	16.3
Ligands	37.25	38.23
Ions	23.5	–
Waters	26.1	23.08
Clashscore	1.30	2.86
Molprobity score	0.99	1.39
Ramachandran plot (%)		
Favored	97.98	95.92
Allowed	1.68	3.06
Outlier	0.34	1.02
RMSD from ideal values		
Bond lengths (Å)	0.0149	0.0103
Bond angles (°)	1.84	1.62
PDB code	9J07	9J08

[a]Values in parentheses represent the highest resolution shell.

forms direct hydrogen bonds with the main chain amides of R76 and N150 and water-mediated hydrogen bonds with D113, Y179, and R224. The interaction with the main chain amides of R76 and N150 corresponds to an oxyanion hole, which plays a key role in the catalysis of α/β-hydrolases (discussed in the 'Active site features' section below).

Structural comparison

A Dali structural similarity search revealed that *Ao*AxeB was most similar to *Lihuaxuella thermophila* poly[(*R*)-3-hydroxybutyric acid] depolymerase (*Lt*PHBase), which belongs to the Esterase_phb family (Table 4) [26]. The second hit was *Acremonium alcalophilum* FAE D (*Aa*FaeD), which belongs to the FaeC family [27]. The third and fourth hits were *Aspergillus sydowii* FAE E (*As*FaeE) [28] and *Al*AxeA [20], respectively, both of which belong to Esterase_phb. The fifth hit was a thermostable esterase A from *Thermotoga maritima* (*Tm*EstA) belonging to the Abhydrolase_5 family [29], which showed significantly lower structural similarity than the four proteins listed above. The overall structures of *Ao*AxeB and its five structural homologs are shown
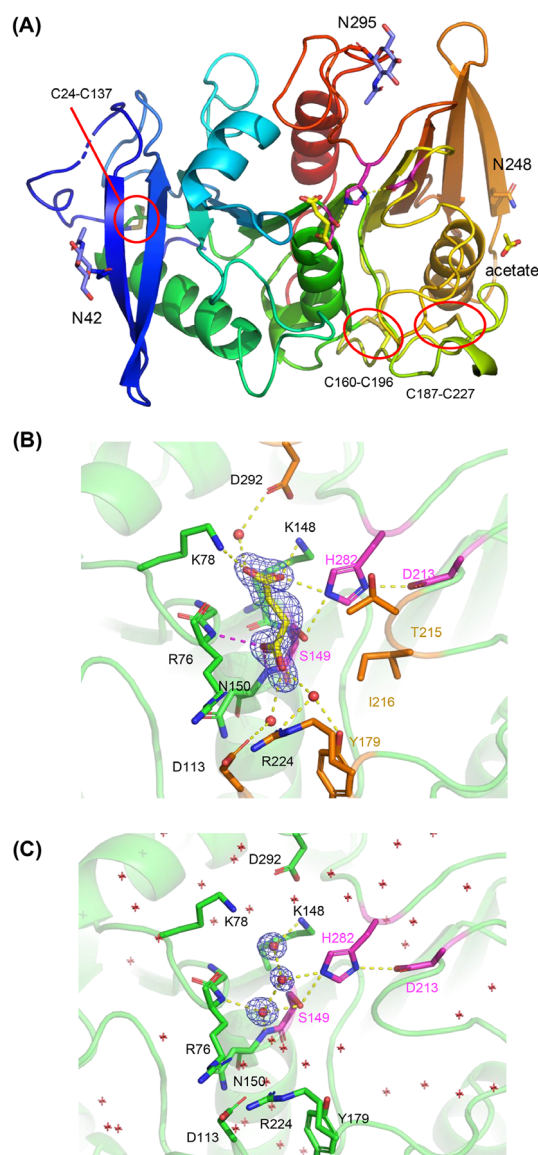
(A)

(B)

(C)

Fig. 3. Crystal structure of *Ao*AxeB. (A) Overall structure. Polypeptide is shown in rainbow colors. N-Glycans (blue), catalytic triad (magenta), disulfide bonds (sulfur atoms in yellow, indicated with red circles), succinate (yellow), and acetate (yellow) are shown as sticks. (B) Active site of the succinate complex structure with a Polder map (4σ). Water atoms and hydrogen bonds are shown as red spheres and yellow dotted lines, respectively. Hydrogen bonds of the oxyanion hole are shown as magenta dotted lines. Residues forming direct hydrogen bonds with succinate and other active site residues are shown as green and orange sticks, respectively. (C) Active site of the apo structure with a Polder map (5σ) for three water molecules near the catalytic center. Other water molecules are shown as red crosshairs. Molecular graphic images were prepared using PYMOL.

in Fig. 5. Interestingly, two of the three disulfide bonds in *Ao*AxeB (C24–C137 and C160–C196) were conserved with *Aa*FaeD in the FaeC family (Fig. 5A,C).

Esterase_phb proteins have a conserved disulfide bond near the catalytic site (C40–C75 in *Al*AxeA, Fig. 5B,D,E) [20], which is not present in *Ao*AxeB. A disulfide bond corresponding to C160–C196 in *Ao*AxeB was also found in *As*FaeE and *Al*AxeA but not in the most structurally similar *Lt*PHBase. There is no disulfide bond in *Tm*EstA belonging to Abhydrolase_5 (Fig. 5F). In summary, *Ao*AxeB has structural features that are intermediate between those of the Esterase_phb and FaeC families. Phylogenetic tree analysis of the amino acid sequences also indicated that *Ao*AxeB was located between two families (Fig. 6).

AXEs and FAEs were also found in distant α/β-hydrolase fold families that were not hit by the structural similarity search with *Ao*FAEB (Table 1). The overall structure of *Ao*AxeB was compared with the distant family enzymes. The central β-sheet of *Ao*AxeB (Fig. 7A) is substantially longer than that of FAE domain of xylanase XynY from *Clostridium thermocellum* (*Ct*Fae-XynY) belonging to Anigen85c family (Fig. 7B) [30] and AXE 1 from *Trichoderma reesei* (*Tr*Axe1) belonging to Cutinase like (and CE5) family (Fig. 7C) [31]. FAE B from *A. oryzae* (*Ao*FaeB) belonging to the Tannase family [32] has additional structural elements around the core α/β-hydrolase and a large lid domain covering the active site (Fig. 7D). FAE A from *Aspergillus niger* (*An*FaeA) [33] belongs to Lipase_3 family, which is categorized in Block L (Table 1). The overall structure of *An*FaeA differs significantly from all other enzymes categorized in Block X (Fig. 7E).

Active site features

The active site of *Ao*AxeB was compared with those of FAEs and AXE (Fig. 8A–D). The structures of *Aa*FaeD and *As*FaeE complexed with ferulic acid showed an open pocket or surrounding pocket for large aromatic compounds (Fig. 8B,C). In contrast, the putative active site of *Ao*AxeB had a small pocket surrounded by R76, R224, Y179, I216, and T215 (Fig. 8A). The pocket size of *Ao*AxeB is similar to that of *Al*AxeA (Fig. 8D). Site-directed mutants of *Al*AxeA in which W160 was replaced by smaller amino acids (Ala, Ser, and Pro) acquired activity against larger aromatic substrates (FAE activity) [20]. This suggested that the small pocket near W160 in *Al*AxeA accommodates an acetyl group of the substrate in AXE activity.

The oxyanion hole is crucial for the catalytic function of serine and cysteine hydrolases and plays a pivotal role in stabilizing the tetrahedral intermediate during the reaction, typically through hydrogen bonding with the backbone amides of the polypeptides [34]. The oxyanion hole of *Ao*AxeB is formed by the main
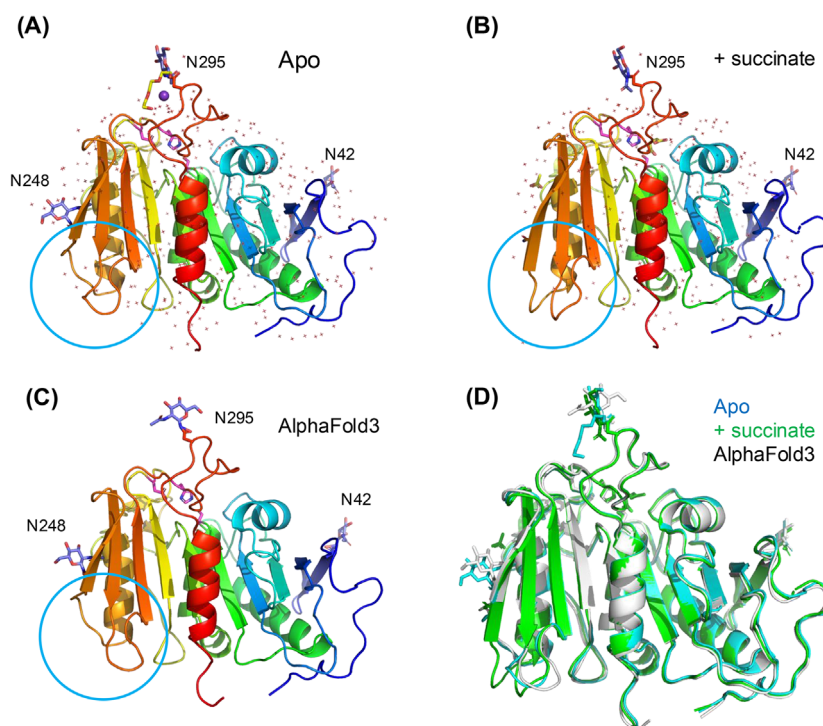
Fig. 4. Comparison of the crystal structures of *Ao*AxeB with predicted structure. (A) Apo structure. A polyethylene glycol molecule (triethylene glycol) and a sodium ion bound on the protein surface are shown as yellow sticks and a purple sphere, respectively. (B) Succinate complex structure. Bound succinate and acetate molecules are shown as yellow sticks. (C) A protein structure (model_0) predicted using the AlphaFold server (beta) [60] on August 1, 2024. The mature protein sequence of *Ao*AxeB (residues 19–326) with N-glycosylation of a single *N*-acetylglucosamine at N42, N248, and N295 was used as a query. The catalytic triad residues are shown as magenta sticks, and water molecules in the crystal structures are shown as red crosshairs. Areas where differences were observed in these structures are circled with cyan. (D) Superimposition of the crystal structures of apo (cyan) and succinate complex (green) forms and the AlphaFold-predicted structure (white). Molecular graphic images were prepared using PYMOL.

Table 4. Result of DALI structural similarity search. Analyzed using the DALI server (http://ekhidna2.biocenter.helsinki.fi/dali/).

Protein	ESTHER[a]	CAZy[b]	PDB ID (chain)	Z score	RMSD (Å)	LALI[c]	%ID[d]
*Lt*PHBase	Esterase_phb	NL	8DAJ (A)	28.8	2.4	253	21
*Aa*FaeD	FaeC	NL	8JH9 (A)	27.9	2.3	234	26
*As*FaeE	Esterase_phb	CE1	8IYb (A)	24.4	2.3	226	21
*Al*AxeA	Esterase_phb	CE1	5X6S (B)	23.8	2.5	229	20
*Tm*EstA	Abhydrolase_5	NL	3DOH (A)	20.8	2.2	206	18

[a]Rank 1 family in the ESTHER database (https://bioweb.supagro.inrae.fr/ESTHER/); [b]Family in the CAZy database (http://www.cazy.org). NL, not listed; [c]Number of aligned residues; [d]Sequence identity.

chain amides of R76 and N150, which form hydrogen bonds with a carboxylate group of succinate (Fig. 8E). This interaction is conserved in *Aa*FaeD and *As*FaeE (Fig. 8F,G) as hydrogen bonds between the carboxylate group in the ferulic acid ligands and the main chain amides of two nearby amino acids are similarly formed.

We performed automated docking analysis to elucidate the substrate-binding mode of *Ao*AxeB. AXEs liberate acetic acid from their esters with 2- or 3-hydroxy groups on the xylan backbone [4]. The deacetylase activity of *Ao*AxeB on acetylated xylooligosaccharides in wheat arabinoxylan is shown (Fig. 2D). Therefore, for the docking analysis, we used xylotriose models acetylated at the 2- or 3-position of the central sugar unit. As a result, plausible binding modes of xylotriose with the *O*-2 and *O*-3 positions of the middle (second) xylose acetylated (2-*O*-Ac²-Xylotriose and 3-*O*-
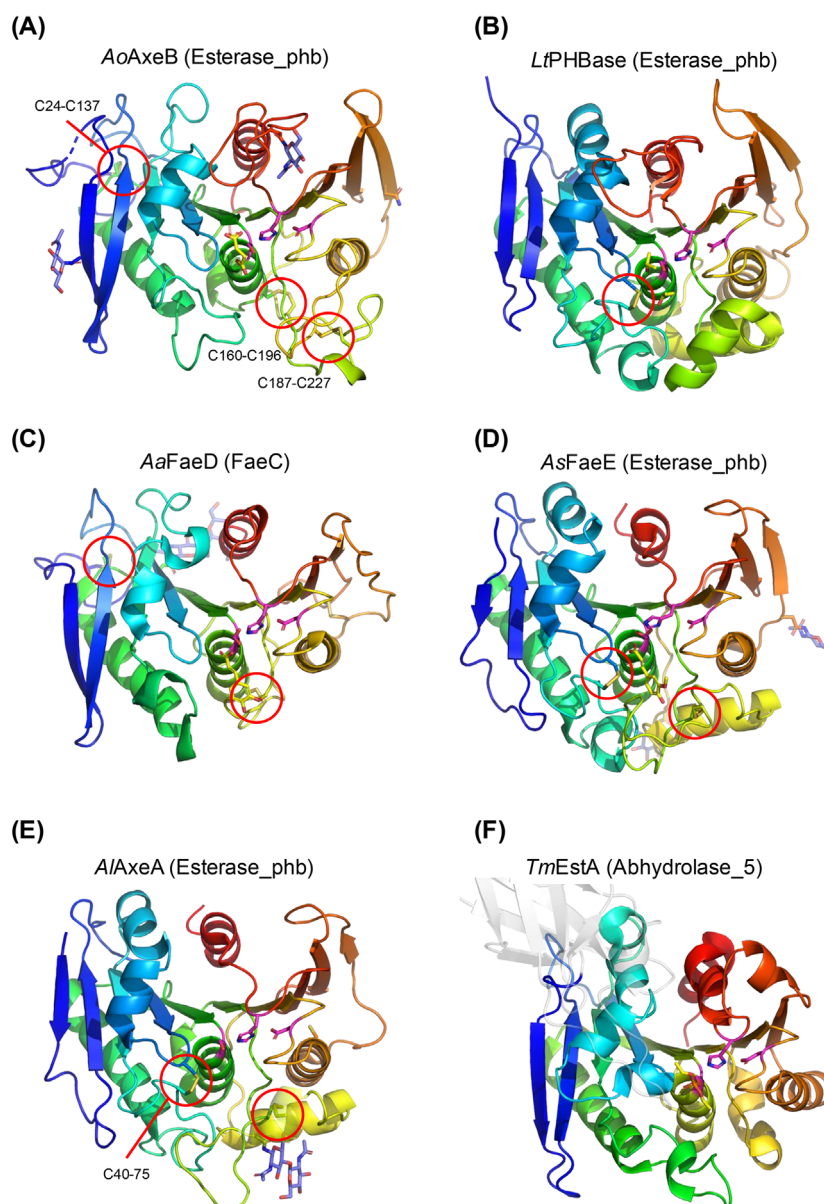
Fig. 5. Structures of *Ao*AxeB and other α/β-hydrolase family enzymes in the top five hits of the structural similarity search. ESTHER family is shown in parentheses. (A) *Ao*AxeB complexed with succinate. (B) *Lihuaxuella thermophila* poly[(*R*)-3-hydroxybutyric acid] depolymerase (*Lt*PHBase) complexed with isopropanol (PDB ID: 8DAJ). (C) *Acremonium alcalophilum* ferulic acid esterase D (*Aa*FaeD) complexed with ferulic acid (PDB ID: 8JH9). (D) *Aspergillus sydowii* ferulic acid esterase E (*As*FaeE) complexed with ferulic acid (PDB ID: 8IYB). (E) *Aspergillus luchuensis* acetyl xylan esterase A (*Al*AxeA, PDB ID: 5X6S). (F) *Thermotoga maritima* thermophilic esterase A (*Tm*EstA) complexed with diethyl phosphate (PDB ID: 3DOI). The N-terminal Ig-like domain is shown transparently in gray. N-glycans (blue), catalytic triad (magenta), disulfide bonds (sulfur atoms in yellow and marked with red circles), and bound ligands (yellow) are shown as sticks. Molecular graphic images were prepared using PYMOL.

Ac^2-Xylotriose) were obtained (Fig. 9). Here we label the xylose units from the nonreducing to reducing ends with −1, 0, and +1, and the acetylated xylose is '0'. The direction of the nonreducing to reducing ends of xylotriose was reversed in 2-*O*-Ac^2-Xylotriose and 3-*O*-Ac^2-Xylotriose. However, the hydrogen bond interactions

with K78, D292, K148, S149, T215, and R223 were conserved. The xylotriose molecules modified at the *O*-2 or *O*-3 positions of the central unit have pseudo-2-fold rotational symmetry, and an example of such oligosaccharides binding to xylanase in both directions has been reported [35]. In 2-*O*-Ac^2-Xylotriose, the O2 and O3 of
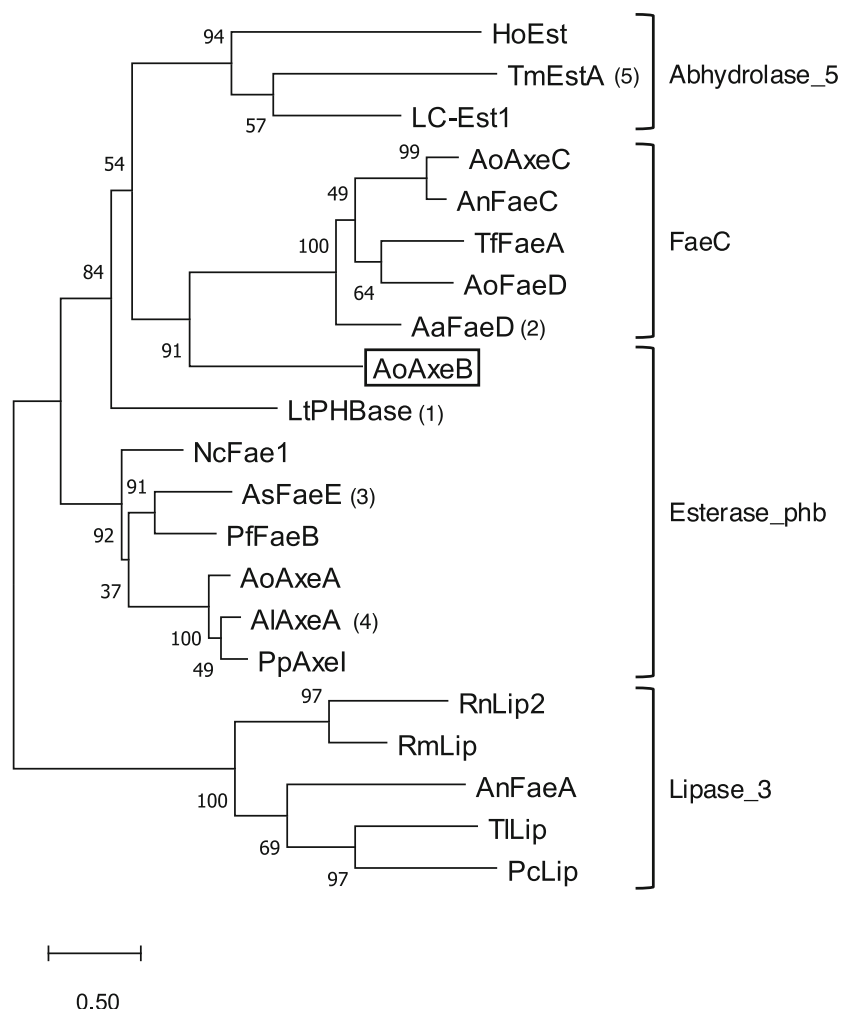
Fig. 6. A phylogenetic tree of esterases in Esterase_phb, FaeC, and Abhydrolase_5 families [58]. The order of structural similarity with *Ao*AxeB is indicated in parentheses. A maximum likelihood tree with the highest log likelihood (−14620.56) is shown. This analysis involved 21 amino acid sequences. Bootstrap values of 200 replications are indicated at the branches. The scale indicates branch lengths measures in the number of substitutions per site. Lipase_3 family members, including *An*FaeA, were included as an outgroup. FaeC, Esterase_phb, and Lipase_3 contain SF5, SF6, and SF7 members in the fungal FAE classification, respectively [59]. The protein names not listed in the text and their ESTHER database IDs are as follows: HoEST, *Haliangium ochraceum* phospholipase/carboxylesterase (halo1-d0lmj0); LC-Est1, a metagenome-derived esterase (9bact-3WYDseq) [61]; AnFaeC, *Aspergillus nidulans* putative ferulic acid esterase (emeni-faec); NcFae1, *Neurospora crassa* Fae-1 (neucr-faeb) [62]; PfFaeB, *Penicillium funiculosum* ferulic acid esterase B (penfn-faeb) [63]; PpAxeI, *Penicillium purpurogenum* acetyl xylan esterase I (penpu-AXEI) [64]; RnLip2, *Rhizopus niveus* lipase II (rhidl-lipas) [65]; RmLip, *Rhizomucor miehei* lipase (rhimi-lipas) [66]; TlLip *Thermomyces lanuginose* lipase (humla-1lipa) [67]; and PcLip *Penicillium camemberti* lipase (penca-mdgli) [68]. Phylogenetic analysis was performed using MEGA software. Details are described in the Materials and methods section.

−1 xylose, the glycosidic bond oxygen linking the −1 and 0 xylose units, and the O2 of +1 xylose are hydrogen bonded to the protein residues (Fig. 9A). In 3-*O*-Ac²-Xylotriose, the O3 of −1 xylose, the glycosidic bond oxygen linking the 0 and +0 xylose units, and the O2 and O3 of +1 xylose are hydrogen bonded to the protein residues (Fig. 9B). Both the 4-hydroxy group at the nonreducing end and the 1-hydroxy group at the reducing end of 2-*O*-Ac²-Xylotriose and 3-*O*-Ac²-

Xylotriose pointed toward the solvent, suggesting that *Ao*AxeB can bind xylooligosaccharides for longer than four sugar units. The acetyl group in the central sugar units of 2-*O*-Ac²-Xylotriose and 3-*O*-Ac²-Xylotriose penetrated the small pocket of the protein, occupying a suitable position under nucleophilic attack by S149 and stabilizing the tetrahedral intermediate by the oxyanion hole. The pocket appears to be able to accommodate an alkyl group with several carbon atoms, but is small
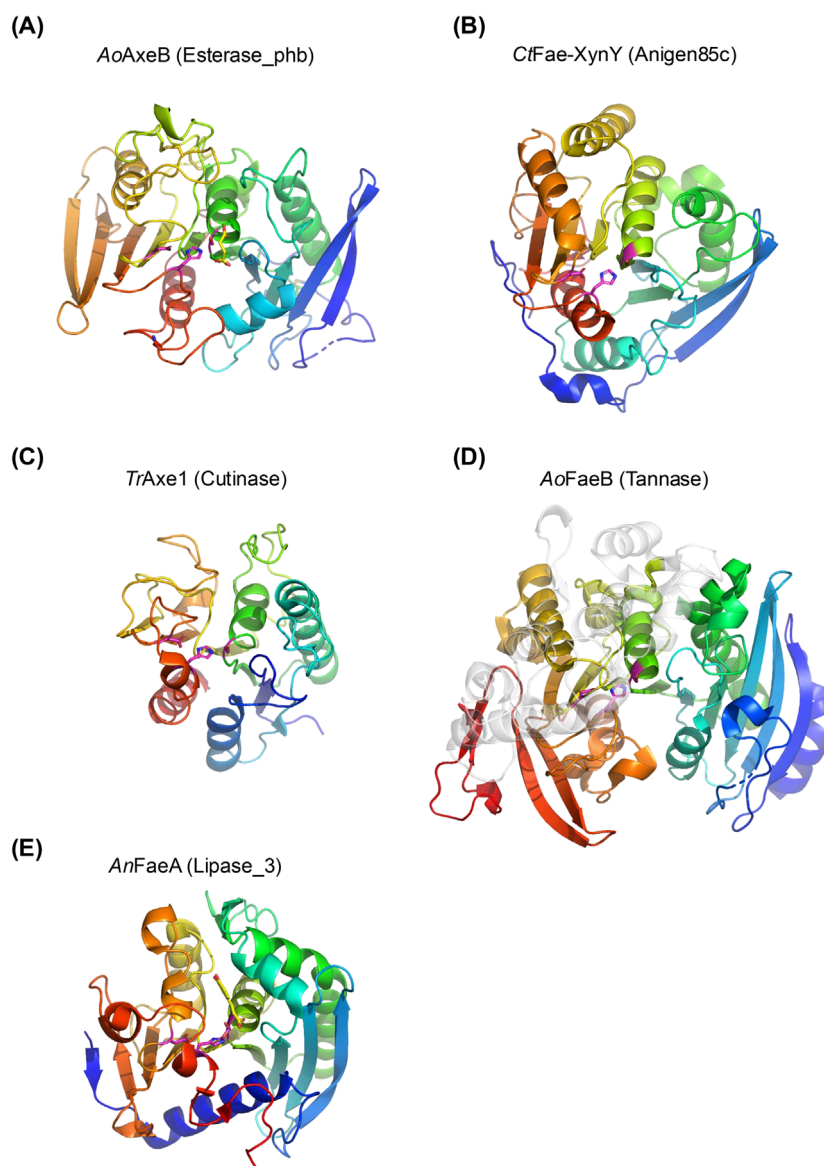
Fig. 7. Structures of *Ao*AxeB and other α/β-hydrolase family acetyl xylan esterases (AXEs) and ferulic acid esterases (FAEs) with lower structural similarity. ESTHER family is shown in parentheses. (A) *Ao*AxeB complexed with succinate. (B) FAE domain of XynY from *Clostridium thermocellum* (*Ct*Fae-XynY, PDB ID: 1GKK). (C) AXE 1 from *Trichoderma reesei* (*Tr*Axe1, PDB ID: 1QOZ). (D) FAE B from *Aspergillus oryzae* (*Ao*FaeB, PDB ID: 3WMT). The lid domain is shown transparently in gray. (E) FAE A from *Aspergillus niger* (*An*FaeA) complexed with ferulic acid (PDB ID: 1UWC). N-glycans (blue), catalytic triad (magenta), and bound ligands (yellow) are shown as sticks. Molecular graphic images were prepared using PYMOL.

enough to favor an acetyl group. Thus, the docking results explained the substrate specificity of *Ao*AxeB (Fig. 2C).

Conclusion

In this study, we discovered and characterized a novel AXE, *Ao*AxeB, from one of the most important industrial microorganisms, *A. oryzae* [36]. Although it has been listed as a putative FAE belonging to Esterase_phb in the ESTHER database, *Ao*AxeB exhibited typical substrate specificity for AXE activity and synergy with xylanase in the deacetylation of wheat arabinoxylan. The crystal structure of *Ao*AxeB revealed that it partly had structural features similar to those of FaeC, and phylogenetic analysis indicated that it was situated between the Esterase_phb and FaeC families. Docking analysis elucidated the possible binding mode
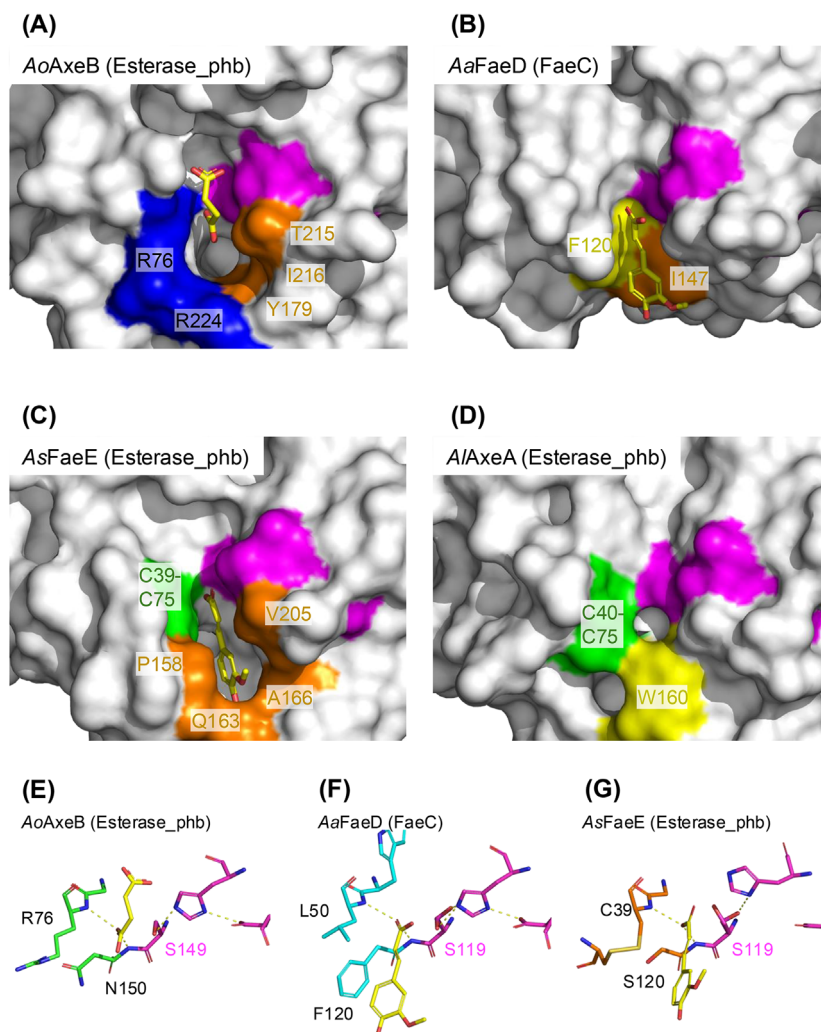
Fig. 8. Active site comparison with ferulic acid esterases (FAEs) and an acetyl xylan esterase (AXE). (A–D) Molecular surface presentations. (A) *Ao*AxeB complexed with succinate. (B) *Aa*FaeD complexed with ferulic acid (PDB ID: 8JH9). (C) *As*FaeE complexed with ferulic acid (PDB ID: 8IYB). (D) *Al*AxeA (PDB ID: 5X6S). The catalytic triad residues are indicated with magenta, and other residues forming the active site pocket are indicated with blue (basic residues), yellow (aromatic residues), green (cysteine residues forming a disulfide bond), or orange (other types of residues). (E–G). The catalytic components of *Ao*AxeB (E, green), *Aa*FaeD (F, cyan), and *As*FaeE (G, orange). Bound ligands (succinate or ferulic acid in yellow), the catalytic triad (magenta), and the oxyanion hole are shown as sticks. Note that the catalytic serine in *Aa*FaeD and AsFaeE takes two alternative conformations, and the catalytic histidine in AsFaeE takes a deviated conformation without forming a hydrogen bond with aspartate. Molecular graphic images were prepared using PYMOL.

of acetylated xylooligosaccharides at the active site. Our study confirmed that there are still unexplored genes for plant cell wall-degrading enzymes in fungal genomes as suggested previously [37].

Materials and methods

Strains and culture conditions

The fungal strains used in the previous report were cultured under similar conditions [19]. *A. oryzae* strain RIB40 and *P. pastoris* strain KM71H were used for the source of the

gene cloning and the heterologous gene expression, respectively. *P. pastoris* transformants were grown at 30 °C in 10 mL of BMGY [1% (w/v) yeast extract, 2% (w/v) peptone, 1% (v/v) glycerol, 0.00004% (w/v) biotin, 1.34% (w/v) yeast nitrogen base with ammonium sulfate, and 10% (v/v) 1 M potassium phosphate (pH 6.0)] medium in a shaking incubator until the cell density reached an OD_{600} of 4. Cells were harvested aseptically by centrifugation (5000 ***g***, 15 min, 4 °C). The cells were then resuspended in 100 mL of BMMY medium [same composition as BMGY medium, except containing 0.5% (v/v) methanol instead of glycerol] in a 500 mL flask to an OD_{600} of 1 to start induction. The
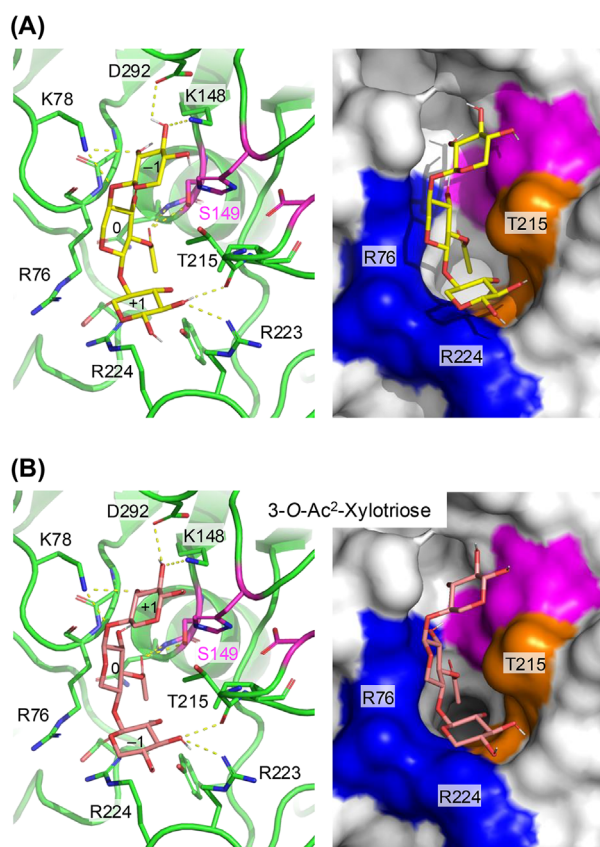
(A)

(B)

Fig. 9. Possible binding modes of acetylated xylooligosaccharides in the active site of *Ao*AxeB. The results of automated docking analysis are shown as the molecular model (left) and surface (right). (A) 2-Acetylated xylotriose (2-*O*-Ac²-Xylotriose, yellow sticks). (B) 3-Acetylated xylotriose (3-*O*-Ac²-Xylotriose, pink sticks). Sugar units from the nonreducing to reducing ends are labeled with −1, 0, and +1. The middle sugar unit labeled '0' is acetylated.

culture was kept in a shaking incubator at 30 °C for 7 days (180 r.p.m.) with the addition of methanol (0.5 mL) once daily to maintain induction.

Cloning and expression of *AoaxeB* gene

The protein-coding sequence of *AoaxeB* from *A. oryzae* (GenBank accession number AO090005000945) was annotated as the hypothetical protein (accession number XP_001817948.1). The protein-coding sequence of *AoaxeB* was amplified using polymerase chain reaction (PCR) with the forward primer 5′-AGGAATTCATGAAGTTTCTCTCAGTAAT-3′ (the *Eco*RI site is underlined), the reverse primer 5′-GTTCTAGACTATCTCGCCTCGCTCTGGT-3′ (the *Xba*I site is underlined), and *A. oryzae* genomic DNA as a template. The PCR products digested with *Eco*RI and *Xba*I were cloned into an *Eco*RI–*Xba*I-digested pPICZB expression vector (Invitrogen, Waltham, MA, USA). The resulting construct pPICZB-AXEB was used to transform

Escherichia coli DH5α, and the positive clone was confirmed using colony PCR. To splice an intron contained within the gene, PCR was performed by inverse PCR using forward primer 5′-AAAGAATGGCAAGGAGACCCA-3′ and reverse primer 5′-GTTGAGCCCCTGCGGGTACAC-3′ with the KOD-Plus-Mutagenesis Kit (TOYOBO, Otsu, Japan). Gene splicing was verified using DNA sequencing. This procedure yielded an expression plasmid vector containing the *AoaxeB* gene with its native signal sequence under the control of the alcohol oxidase 1 (*aox1*) promoter and terminator for expression in *P. pastoris* as described above.

Purification of recombinant *Ao*AxeB

Recombinant proteins were expressed and purified by a procedure similar to the previous report [19]. The recombinant plasmid (pPICZB-AXEB) was linearized with *Pme*I and subsequently transformed into *P. pastoris* KH71H using the Pichia EasyComp Transformation Kit (Invitrogen) according to the manufacturer's protocol. The 7-days cell culture was harvested by centrifugation (5000 ***g***, 15 min). The culture supernatant was used for the purification of recombinant *Ao*AxeB. Enzyme purification was performed as previously described [19]. The cell culture was harvested by centrifugation (5000 ***g***, 15 min). The culture supernatants of recombinant *Ao*AxeB were applied to a DEAE-5PW anion-exchange column (15 mm × 15 cm; Tosoh Co., Tokyo, Japan) equilibrated with 50 mM sodium phosphate buffer (pH 7.0) using high-performance liquid chromatography (HPLC; Shimadzu, Tokyo, Japan). Proteins were eluted with a linear gradient in NaCl (0–0.4 M) in 50 mM sodium phosphate buffer (pH 7.0) at a flow rate of 3 mL·min^{-1}. Fractions containing esterase activity were collected, pooled, concentrated by ultrafiltration, and subsequently applied to an ENrich SEC650 gel filtration column (10 × 300 mm; Bio-Rad, Hercules, CA, USA) using the ÄKTA fast protein liquid chromatography purification system (ÄKTApurifier UPC10; Cytiva, Tokyo, Japan). The column was eluted in 1 mL fractions with 50 mM sodium phosphate buffer (pH 7.0) containing 0.15 M NaCl at a flow rate of 1.0 mL·min^{-1}. Enzyme purity and molecular mass were evaluated using 12% SDS/PAGE, followed by Coomassie Brilliant Blue staining. The protein concentration was measured using a Micro BCA Protein Assay Kit (Thermo Fisher Scientific Inc., Waltham, MA, USA). After boiling, the purified *Ao*AxeB protein was treated with 0.5 mU of Endo-H (FUJIFILM Wako Pure Chemical Industries, Osaka, Japan) in 50 mM sodium acetate buffer (pH 5.0) at 37 °C for 18 h.

Assay of enzyme activity

The activity of purified *Ao*AxeB toward wheat arabinoxylan, α-naphthyl acetate (C2), propionate (C3), butyrate (C4), caprylate (C8), laurate (C12), palmitate (C16), methyl ferulate, methyl *p*-coumarate, methyl caffeate, and methyl sinapate was investigated under a similar condition

to the previous report [19]. The synthetic α-naphthyl and methyl substrates have been used as model substrates for AXEs and FAEs [19–21,38,39]. Esterase activity was assayed as follows: α-naphthyl esters dissolved in dimethyl sulfoxide were added to 0.9 mL of 50 mM sodium phosphate buffer (pH 8.0), at a final concentration of 5 mM, and 0.1 mL of enzyme source (0.46 mg·mL^{-1}) was then added. For control reactions, 0.1 mL of H$_2$O was used instead of the enzyme solution. Although α-naphthyl esters are unstable under alkaline conditions (pH ≥ 8), they were relatively stable when phosphate buffer was used (Fig. S1), and nonenzymatic degradation was subtracted to calculate the enzyme activity. The reaction mixture was incubated for 15 min at 30 °C and terminated by the addition of 0.5 mL of 15% (wt/vol) sodium dodecyl sulfate containing 0.1% (wt/vol) Fast Garnet GBC (Sigma-Aldrich, St. Louis, MO, USA). After incubation at room temperature for 15 min, the optical density at 560 nm was measured. The standard curve was prepared by using α-naphthol. One unit (U) of the enzyme activity was defined as the amount of enzyme that releases 1 μmol of α-naphthol·min^{-1} under the above assay conditions. The activity as a function of pH for the α-naphthyl acetate substrate was measured using citrate buffer (pH 5.0–6.0), phosphate buffer (pH 6.0–8.0), and Tris/HCl buffer (pH 8.0–9.0) at 30 °C. The activity as a function of temperature in the range 30–55 °C, using increments of 5.0 °C, was performed in 50 mM sodium phosphate (pH 8.0). To measure the thermal stability of *Ao*AxeB, the enzyme was incubated at an appropriate temperature for 1 h, and residual activity was determined using α-naphthyl acetate as the substrate.

Release of acetic acid from acetylated xylan and synergism with xylanase

The activity of *Ao*AxeB toward acetylated xylan was assayed under similar conditions to the previous reports [19,40]. Insoluble wheat arabinoxylan (Megazyme, Braw, Wicklow, Ireland) was used as substrate at a final concentration of 2.0% and in a final volume of 4.0 mL at 37 °C for 6 h in 50 mM phosphate buffer (pH 8.0) with purified protein (60 μg). The amount of acetic acid released was determined using an F-kit acetate kit (Roche, Basel, Switzerland). The synergistic effect between *Ao*AxeB and *Tl*Xyn (Sigma-Aldrich) was investigated by incubation of a 4 mL solution of 2.0% insoluble wheat arabinoxylan (Sigma-Aldrich) in 50 mM phosphate buffer (pH 8.0) for 4 h at 37 °C with purified *Ao*AxeB (60 μg) and *Tl*Xyn (10 μg, ≥ 2500 units·g^{-1}). The synergistic effect was determined based on the amount of acetic acid released using an acetic acid assay kit (Roche).

Crystallization and structure determination

The crystals of *Ao*AxeB were obtained at 20 °C using the sitting-drop vapor diffusion method by mixing equal volumes of protein and reservoir solutions. For apo-form crystals, a protein solution containing 2 mg·mL^{-1} *Ao*AxeB and 10 mM xylooligosaccharides (FUJIFILM Wako Pure Chemical Industries) and a reservoir solution containing 0.2 M potassium fluoride and 20% PEG3350 (w/v) were used. The electron densities of the xylooligosaccharides were not observed in the resulting crystal structure. For succinate complex crystals, protein solution containing 3 mg·mL^{-1} *Ao*AxeB and reservoir solution containing 0.1 M sodium acetate buffer (pH 4.5) and 20% (w/v) PEG3000 were used. For data collection, the crystals were cryoprotected using a reservoir solution supplemented with 20% (v/v) PEG200 and flash-cooled by dipping in liquid nitrogen. X-ray diffraction data were collected at 100 K on the beamlines at the Photon Factory of the High Energy Accelerator Research Organization (KEK, Tsukuba, Japan) and the Swiss Light Source (SLS) of the Paul Scherrer Institut (PSI) (Villigen, Switzerland). The preliminary diffraction data were collected at SPring-8 (Hyogo, Japan). The datasets were processed using the XDS [41] and AIMLESS software [42]. The initial phase was obtained through molecular replacement using MORDA [43] with the LC-Est1 structure (PDB ID: 3WYD, chain A) as a template. Phase improvement and automated model building were achieved using PHENIX (phase and build) [44] and BUCCANEER software [45]. Manual model rebuilding and refinement were performed using COOT [46] and REFMAC5 [47]. Polder maps were prepared using PHENIX software [48]. Molecular graphic images were prepared using PYMOL (Schrödinger LLC, New York, NY, USA).

Phylogenetic and docking analyses

Phylogenetic analysis was performed using MEGA 11.0.13 [49]. The protein sequences were aligned using MUSCLE [50]. The docking study was performed using AUTODOCK VINA 1.2.5 [51]. Using AutoDockTools, polar hydrogen atoms were added to the amino acid residues, and Gasteiger charges were assigned to all atoms of the enzyme. The grid map was prepared with 20 × 20 × 20 points spaced at 1.0 Å distances. The grid box was centered on the carboxy carbon atom of succinate near the catalytic serine of *Ao*AxeB. The exhaustiveness value is 256. The ligand structure was docked at flexible torsion angles, whereas the protein structure was fixed. Docking of 2-*O*-Ac^2-Xylotriose yielded nine binding modes with estimated affinities ranging from −6.958 to −6.336 kcal·mol^{-1}, with the second-best result (−6.893 kcal·mol^{-1}) being selected. The result with the lowest estimated affinity was catalytically irrelevant. Docking of 3-*O*-Ac^2-Xylotriose yielded eight binding modes with estimated affinities ranging −7.299 to −6.338 kcal·mol^{-1}, with the second-best result (−6.893 kcal·mol^{-1}) being selected. The first-ranked docking result was not catalytically competent for either ligand.

Acknowledgements

Conflicts of interest

The authors declare no conflict of interest.

Author contributions

TKo, SF, and YS conceived and supervised the study; CY, TKo, and SF planned experiments; CY, TKa, and TKo performed experiments; TKa and TKo performed the protein production, purification, and biochemical experiments; CY and SF performed protein crystallography; SF performed the phylogenetic and docking analyses; and TKo and SF wrote the manuscript. All authors reviewed the final version of the manuscript.

Peer review

The peer review history for this article is available at https://www.webofscience.com/api/gateway/wos/peer-review/10.1111/febs.17420.

Data availability statement

Atomic coordinates and structure factors of the crystal structures have been deposited in the Protein Data Bank under accession numbers 9J07 and 9J08. The source data are provided in this paper.

References

1 Scheller HV & Ulvskov P (2010) Hemicelluloses. *Annu Rev Plant Biol* **61**, 263–289.

2 Biely P (2012) Microbial carbohydrate esterases deacetylating plant polysaccharides. *Biotechnol Adv* **30**, 1575–1588.

3 Biely P, Westereng B, Puchart V, de Maayer P & Cowan DA (2014) Recent progress in understanding the mode of action of acetylxylan esterases. *J Appl Glycosci* **61**, 35–44.

4 Puchart V & Biely P (2023) Microbial xylanolytic carbohydrate esterases. *Essays Biochem* **67**, 479–491.

5 Nardini M & Dijkstra BW (1999) α/β Hydrolase fold enzymes: the family keeps growing. *Curr Opin Struct Biol* **9**, 732–737.

6 Chatonnet A, Perochon M, Velluet E & Marchot P (2023) The ESTHER database on alpha/beta hydrolase fold proteins – an overview of recent developments. *Chem Biol Interact* **383**, 110671.

7 Drula E, Garron ML, Dogan S, Lombard V, Henrissat B & Terrapon N (2022) The carbohydrate-active enzyme database: functions and literature. *Nucleic Acids Res* **50**, D571–D577.

8 Adesioye FA, Makhalanyane TP, Biely P & Cowan DA (2016) Phylogeny, classification and metagenomic bioprospecting of microbial acetyl xylan esterases. *Enzyme Microb Technol* **93–94**, 79–91.

9 Li X, Griffin K, Langeveld S, Frommhagen M, Underlin EN, Kabel MA, de Vries RP & Dilokpimol A (2020) Functional validation of two fungal subfamilies in carbohydrate esterase family 1 by biochemical characterization of esterases from uncharacterized branches. *Front Bioeng Biotechnol* **8**, 542687.

10 Chung HJ, Park SM, Kim HR, Yang MS & Kim DH (2002) Cloning the gene encoding acetyl xylan esterase from *Aspergillus ficuum* and its expression in *Pichia pastoris*. *Enzyme Microb Technol* **31**, 384–391.

11 Koseki T, Furuse S, Iwano K, Sakai H & Matsuzawa H (1997) An *Aspergillus awamori* acetylesterase: purification of the enzyme, and cloning and sequencing of the gene. *Biochem J* **326**, 485–490.

12 Koseki T, Miwa Y, Akao T, Akita O & Hashizume K (2006) An *Aspergillus oryzae* acetyl xylan esterase: molecular cloning and characteristics of recombinant enzyme expressed in *Pichia pastoris*. *J Biotechnol* **121**, 381–389.

13 Bauer S, Vasu P, Persson S, Mort AJ & Somerville CR (2006) Development and application of a suite of polysaccharide-degrading enzymes for analyzing plant cell walls. *Proc Natl Acad Sci USA* **103**, 11417–11422.

14 Puchart V, Agger JW, Berrin JG, Várnai A, Westereng B & Biely P (2016) Comparison of fungal carbohydrate esterases of family CE16 on artificial and natural substrates. *J Biotechnol* **233**, 228–236.

15 Zhang Y, Ding HT, Jiang WX, Zhang X, Cao HY, Wang JP, Li CY, Huang F, Zhang XY, Chen XL *et al.* (2021) Active site architecture of an acetyl xylan esterase indicates a novel cold adaptation strategy. *J Biol Chem* **297**, 100841.

16 Akoh CC, Lee GC, Liaw YC, Huang TH & Shaw JF (2004) GDSL family of serine esterases/lipases. *Prog Lipid Res* **43**, 534–552.

17 Correia MAS, Prates JAM, Brás J, Fontes CMGA, Newman JA, Lewis RJ, Gilbert HJ & Flint JE (2008) Crystal structure of a cellulosomal family 3 carbohydrate esterase from *Clostridium thermocellum* provides insights into the mechanism of substrate recognition. *J Mol Biol* **379**, 64–72.

18 Montanier C, Money VA, Pires VMR, Flint JE, Pinheiro BA, Goyal A, Prates JAM, Izumi A, Stålbrand H, Morland C *et al.* (2009) The active site of a carbohydrate esterase displays divergent catalytic and noncatalytic binding functions. *PLoS Biol* **7**, e1000071.

19 Kato T, Shiono Y & Koseki T (2021) Identification and characterization of an acetyl xylan esterase from *Aspergillus oryzae*. *J Biosci Bioeng* **132**, 337–342.

20 Komiya D, Hori A, Ishida T, Igarashi K, Samejima M, Koseki T & Fushinobu S (2017) Crystal structure and substrate specificity modification of acetyl xylan esterase from *Aspergillus luchuensis*. *Appl Environ Microbiol* **83**, e01251-17.

21 Koseki T, Handa H, Watanabe Y, Ohtsuka M & Shiono Y (2016) An unusual feruloyl esterase from *Aspergillus oryzae*: two tryptophan residues play a crucial role for the activity. *J Mol Catal B Enzym* **133**, S560–S568.

22 Gupta R & Brunak S (2002) Prediction of glycosylation across the human proteome and the correlation to protein function. *Pac Symp Biocomput* **7**, 310–322.

23 Singh S, Madlala AM & Prior BA (2003) *Thermomyces lanuginosus*: properties of strains and their hemicellulases. *FEMS Microbiol Rev* **27**, 3–16.

24 Kojima K, Sunagawa N, Yoshimi Y, Tryfona T, Samejima M, Dupree P & Igarashi K (2022) Acetylated xylan degradation by glycoside hydrolase family 10 and 11 xylanases from the white-rot fungus *Phanerochaete chrysosporium*. *J Appl Glycosci* **69**, 35–43.

25 Krissinel E & Henrick K (2007) Inference of macromolecular assemblies from crystalline state. *J Mol Biol* **372**, 774–797.

26 Thomas GM, Quirk S, Huard DJE & Lieberman RL (2022) Bioplastic degradation by a polyhydroxybutyrate depolymerase from a thermophilic soil bacterium. *Protein Sci* **31**, e4470.

27 Phienluphon A, Kondo K, Mikami B, Teo KSK, Saito K, Watanabe T, Nagata T & Katahira M (2024) Structure-based characterization and improvement of an enzymatic activity of *Acremonium alcalophilum* feruloyl esterase. *ACS Sustain Chem Eng* **12**, 3831–3840.

28 Phienluphon A, Kondo K, Mikami B, Nagata T & Katahira M (2023) Structural insights into the molecular mechanisms of substrate recognition and hydrolysis by feruloyl esterase from *Aspergillus sydowii*. *Int J Biol Macromol* **253**, 127188.

29 Levisson M, Sun L, Hendriks S, Swinkels P, Akveld T, Bultema JB, Barendregt A, van den Heuvel RHH, Dijkstra BW, van der Oost J *et al.* (2009) Crystal structure and biochemical properties of a novel thermostable esterase containing an immunoglobulin-like domain. *J Mol Biol* **385**, 949–962.

30 Prates JAM, Tarbouriech N, Charnock SJ, Fontes CMGA, Ferreira LMA & Davies GJ (2001) The structure of the feruloyl esterase module of xylanase 10B from *Clostridium thermocellum* provides insights into substrate recognition. *Structure* **9**, 1183–1190.

31 Hakulinen N, Tenkanen M & Rouvinen J (2000) Three-dimensional structure of the catalytic core of acetylxylan esterase from *Trichoderma reesei*: insights into the deacetylation mechanism. *J Struct Biol* **132**, 180–190.

32 Suzuki K, Hori A, Kawamoto K, Thangudu RR, Ishida T, Igarashi K, Samejima M, Yamada C, Arakawa T, Wakagi T *et al.* (2014) Crystal structure of a feruloyl esterase belonging to the tannase family: a disulfide bond near a catalytic triad. *Proteins* **82**, 2857–2867.

33 McAuley KE, Svendsen A, Patkar SA & Wilson KS (2004) Structure of a feruloyl esterase from *Aspergillus niger*. *Acta Crystallogr D* **60**, 878–887.

34 Berg JM, Gatto GJ, Hines J, Tymoczko JL & Stryer L (2023) 6. Enzyme catalytic strategies. In Biochemistry, 10th edn, pp. 179–209. W. H. Freeman, San Francisco, CA.

35 Fujimoto Z, Kaneko S, Kuno A, Kobayashi H, Kusakabe I & Mizuno H (2004) Crystal structures of decorated xylooligosaccharides bound to a family 10 xylanase from *Streptomyces olivaceoviridis* E-86. *J Biol Chem* **279**, 9606–9614.

36 Ichishima E (2016) Development of enzyme technology for *Aspergillus oryzae*, *A. sojae*, and *A. luchuensis*, the national microorganisms of Japan. *Biosci Biotechnol Biochem* **80**, 1681–1692.

37 Choi J, Kim KT, Jeon J & Lee YH (2013) Fungal plant cell wall-degrading enzyme database: a platform for comparative and evolutionary genomics in fungi and oomycetes. *BMC Genomics* **14**, S7.

38 Faulds CB & Williamson G (1994) Purification and characterization of a ferulic acid esterase (FAE-III) from *Aspergillus niger*: specificity for the phenolic moiety and binding to microcrystalline cellulose. *Microbiology* **140**, 779–787.

39 Koseki T, Miwa Y, Fushinobu S & Hashizume K (2005) Biochemical characterization of recombinant acetyl xylan esterase from *Aspergillus awamori* expressed in *Pichia pastoris*: mutational analysis of catalytic residues. *Biochim Biophys Acta* **1749**, 7–13.

40 Koseki T, Takahashi K, Fushinobu S, Iefuji H, Iwano K, Hashizume K & Matsuzawa H (2005) Mutational

analysis of a feruloyl esterase from *Aspergillus awamori* involved in substrate discrimination and pH dependence. *Biochim Biophys Acta* **1722**, 200–208.

41 Kabsch W (2010) XDS. *Acta Crystallogr D* **66**, 125–132.

42 Evans PR & Murshudov GN (2013) How good are my data and what is the resolution? *Acta Crystallogr D* **69**, 1204–1214.

43 Vagin A & Lebedev A (2015) MoRDa, an automatic molecular replacement pipeline. *Acta Crystallogr A* **71**, s19.

44 Liebschner D, Afonine PV, Baker ML, Bunkoczi G, Chen VB, Croll TI, Hintze B, Hung LW, Jain S, McCoy AJ *et al.* (2019) Macromolecular structure determination using X-rays, neutrons and electrons: recent developments in Phenix. *Acta Crystallogr D* **75**, 861–877.

45 Cowtan K (2006) The Buccaneer software for automated model building. 1. Tracing protein chains. *Acta Crystallogr D* **62**, 1002–1011.

46 Emsley P, Lohkamp B, Scott WG & Cowtan K (2010) Features and development of Coot. *Acta Crystallogr Sect D-Struct Biol* **66**, 486–501.

47 Murshudov GN, Skubák P, Lebedev AA, Pannu NS, Steiner RA, Nicholls RA, Winn MD, Long F & Vagin AA (2011) REFMAC5 for the refinement of macromolecular crystal structures. *Acta Crystallogr D* **67**, 355–367.

48 Liebschner D, Afonine PV, Moriarty NW, Poon BK, Sobolev OV, Terwilliger TC & Adams PD (2017) Polder maps: improving OMIT maps by excluding bulk solvent. *Acta Crystallogr D* **73**, 148–157.

49 Tamura K, Stecher G & Kumar S (2021) MEGA11: molecular evolutionary genetics analysis version 11. *Mol Biol Evol* **38**, 3022–3027.

50 Edgar RC (2004) MUSCLE: multiple sequence alignment with high accuracy and high throughput. *Nucleic Acids Res* **32**, 1792–1797.

51 Eberhardt J, Santos-Martins D, Tillack AF & Forli S (2021) AutoDock Vina 1.2.0: new docking methods, expanded force field, and Python bindings. *J Chem Inf Model* **61**, 3891–3898.

52 Martinez C, De Geus P, Lauwereys M, Matthyssens G & Cambillau C (1992) *Fusarium solani* cutinase is a lipolytic enzyme with a catalytic serine accessible to solvent. *Nature* **356**, 615–618.

53 Ghosh D, Sawicki M, Lala P, Erman M, Pangborn W, Eyzaguirre J, Gutiérrez R, Jörnvall H & Thiel DJ (2001) Multiple conformations of catalytic serine and histidine in acetylxylan esterase at 0.90 Å. *J Biol Chem* **276**, 11159–11166.

54 Montoro-García S, Gil-Ortiz F, García-Carmona F, Polo LM, Rubio V & Sánchez-Ferrer Á (2011) The crystal structure of the cephalosporin deacetylating

enzyme acetyl xylan esterase bound to paraoxon explains the low sensitivity of this serine hydrolase to organophosphate inactivation. *Biochem J* **436**, 321–330.

55 Hatamoto O, Watarai T, Kikuchi M, Mizusawa K & Sekine H (1996) Cloning and sequencing of the gene encoding tannase and a structural study of the tannase subunit from *Aspergillus oryzae*. *Gene* **175**, 215–221.

56 Yoshida S, Hiraga K, Takehana T, Taniguchi I, Yamaji H, Maeda Y, Toyohara K, Miyamoto K, Kimura Y & Oda K (2016) A bacterium that degrades and assimilates poly(ethylene terephthalate). *Science* **351**, 1196–1199.

57 Goldstone DC, Villas-Bôas SG, Till M, Kelly WJ, Attwood GT & Arcus VL (2010) Structural and functional characterization of a promiscuous feruloyl esterase (Est1E) from the rumen bacterium *Butyrivibrio proteoclasticus*. *Proteins* **78**, 1457–1469.

58 Matoba Y, Tanaka N, Noda M, Higashikawa F, Kumagai T & Sugiyama M (2013) Crystallographic and mutational analyses of tannase from *Lactobacillus plantarum*. *Proteins* **81**, 2052–2058.

59 Dilokpimol A, Mäkelä MR, Aguilar-Pontes MV, Benoit-Gelber I, Hildén KS & De Vries RP (2016) Diversity of fungal feruloyl esterases: updated phylogenetic classification, properties, and industrial applications. *Biotechnol Biofuels* **9**, 231.

60 Abramson J, Adler J, Dunger J, Evans R, Green T, Pritzel A, Ronneberger O, Willmore L, Ballard AJ, Bambrick J *et al.* (2024) Accurate structure prediction of biomolecular interactions with AlphaFold 3. *Nature* **630**, 493–500.

61 Okano H, Hong X, Kanaya E, Angkawidjaja C & Kanaya S (2015) Structural and biochemical characterization of a metagenome-derived esterase with a long N-terminal extension. *Protein Sci* **24**, 93–104.

62 Crepin VF, Faulds CB & Connerton IF (2003) A non-modular type B feruloyl esterase from *Neurospora crassa* exhibits concentration-dependent substrate inhibition. *Biochem J* **370**, 417–427.

63 Kroon PA, Williamson G, Fish NM, Archer DB & Belshaw NJ (2000) A modular esterase from *Penicillium funiculosum* which releases ferulic acid from plant cell walls and binds crystalline cellulose contains a carbohydrate binding module. *Eur J Biochem* **267**, 6740–6752.

64 Gordillo F, Caputo V, Peirano A, Chavez R, Van Beeumen J, Vandenberghe I, Claeyssens M, Bull P, Ravanal MC & Eyzaguirre J (2006) *Penicillium purpurogenum* produces a family 1 acetyl xylan esterase containing a carbohydrate-binding module: characterization of the protein and its gene. *Mycol Res* **110**, 1129–1139.

65 Kohno M, Funatsu J, Mikami B, Kugimiya W, Matsuo T & Morita Y (1996) The crystal structure of lipase II

from *Rhizopus niveus* at 2.2 Å resolution. *J Biochem* **120**, 505–510.

66 Brady L, Brzozowski AM, Derewenda ZS, Dodson E, Dodson G, Tolley S, Turkenburg JP, Christiansen L, Huge-Jensen B, Norskov L *et al.* (1990) A serine protease triad forms the catalytic centre of a triacylglycerol lipase. *Nature* **343**, 767–770.

67 Brzozowski AM, Savage H, Verma CS, Turkenburg JP, Lawson DM, Svendsen A & Patkar S (2000) Structural origins of the interfacial activation in *Thermomyces* (*Humicola*) *lanuginosa* lipase. *Biochemistry* **39**, 15071–15082.

68 Derewenda U, Swenson L, Green R, Wei Y, Dodson GG, Yamaguchi S, Haas MJ & Derewenda ZS (1994) An unusual buried polar cluster in a family of fungal lipases. *Nat Struct Biol* **1**, 36–47.

Supporting information

Additional supporting information may be found online in the Supporting Information section at the end of the article.

Fig. S1. Effect of pH on the hydrolytic activity of α-naphthyl acetate (αNA) by purified recombinant *Ao*AxeB.